Published in final edited form as:

Nat Struct Mol Biol. 2013 May ; 20(5): 582–588. doi:10.1038/nsmb.2544.

Dynamics of translation by single ribosomes through mRNA secondary structures

Chunlai Chen[1], **Haibo Zhang**[2], **Steven L. Broitman**[3], **Michael Reiche**[2], **Ian Farrell**[2,4], **Barry S. Cooperman**[2], and **Yale E. Goldman**[1]

[1]Pennsylvania Muscle Institute, Perelman School of Medicine, University of Pennsylvania, Philadelphia, Pennsylvania, USA

[2]Department of Chemistry, University of Pennsylvania, Philadelphia, Pennsylvania, USA

[3]Cell & Molecular Biology, Department of Biology, West Chester University of Pennsylvania, West Chester, Pennsylvania, USA

[4] Anima Cell Metrology, Inc., Bernardsville, New Jersey, USA

Abstract

During protein synthesis, the ribosome translates nucleotide triplets in single-stranded mRNA into polypeptide sequences. Strong downstream mRNA secondary (2°) structures, which must be unfolded for translation, can slow or even halt protein synthesis. Here we employ single molecule fluorescence resonance energy transfer to determine reaction rates for specific steps within the elongation cycle as the *Escherichia coli* ribosome encounters stem loop or pseudoknot mRNA 2° structures. Downstream stem-loops containing 100% G-C base pairs decrease the rates of both tRNA translocation within the ribosome and deacylated tRNA dissociation from the ribosomal exit (E) site. Downstream stem-loops or pseudoknots containing both G-C and A-U pairs also decrease the rate of tRNA dissociation, but they have little effect on tRNA translocation rate. Thus, somewhat surprisingly, unfolding of mRNA 2° structures is more closely coupled to E-site tRNA dissociation than to tRNA translocation.

Introduction

Polypeptide elongation by the ribosome proceeds discontinuously [1-3], with pauses regulating the rhythm of protein synthesis. Translation rates are known to be modulated by mRNA secondary structures downstream of the decoding center. Downstream pseudoknots or stem-loops, which have to be unfolded by the ribosome in order to be translated, can slow or even halt protein synthesis. Such pauses have been linked functionally to co-translational protein folding [4], protein modification, and frame-shifts. Programmed frameshifting [5,6], which is

Correspondence should be addressed to: B.S.C (cooprman@pobox.upenn.edu) and Y.E.G (goldmany@mail.med.upenn.edu).

Author Contributions

C.C., B.S.C. and Y.E.G. designed the experiments. C.C., S.L.B. and M.R. conducted the experiments and analyzed the data. H.Z. and I.F. prepared reagents. C.C., B.S.C. and Y.E.G. wrote the paper.

often required for viral pathogenicity, is usually associated with 'slippery' oligonucleotide sequences acting in conjunction with pseudoknots [7]. In some cases stem-loops can also induce frameshifting [8,9].

The ribosome contains an mRNA entry channel which is believed to admit only single stranded RNA [10], thereby ensuring that bases in the mRNA are exposed for codon-anticodon interactions with aminoacylated-tRNA (aa-tRNA). Secondary (2°) structures such as pseudoknots or stem-loops are unwound by the ribosome's intrinsic helicase activity [11]. For prokaryotic ribosomes, proteins S3, S4 and S5, which encircle the entrance to the mRNA channel, are implicated in helicase activity. Homologous proteins are present in eukaryotic ribosomes [12].

An elongation cycle of polypeptide synthesis can be divided into three major kinetic steps: i) binding and codon-dependent recognition of the incoming aa-tRNA to the aminoacyl-site (A-site) followed rapidly by peptide bond formation, resulting in formation of a pretranslocation (PRE) complex with peptidyl-tRNA bound in the A-site and deacylated tRNA bound in the peptidyl-site (P-site), ii) translocation to form a posttranslocation (POST) complex with deacylated tRNA bound in the exit site (E-site) and peptidyl-tRNA bound in the P-site and, iii) dissociation of the deacylated tRNA from the E-site. Here we present single molecule fluorescence resonance energy transfer (smFRET) and related ensemble measurements of these steps as modulated by downstream mRNA 2° structures.

Single molecule measurements have the advantage of monitoring the reaction pathways of individual ribosomes, avoiding the inevitable loss of dynamic information that occurs in averaging ensemble measurements [13]. Recent optical trap studies have directly demonstrated the slowing of translation caused by very large mRNA duplexes [14,15] but how the elongation is modulated by mRNA 2° structures more closely resembling those found in Nature and how dynamics within individual elongation cycles are altered have heretofore been unknown. To elucidate the mechanisms by which mRNA 2° structures slow translation, we determined, for the first time, the kinetics of the three major sub-steps within each elongation cycle when downstream mRNA 2° structures are unwound.

RESULTS

Design of the smFRET experiments

We inserted several mRNA 2° structures downstream from a common sequence coding for the peptide $^{f}M(YE)_3R^8F^9V^{10}$ (single letter amino acid code) (Fig. 1 and Supplementary Table 1). mRNA mPL has the least stable 2° structure. mRNAs mSL-15, mSL-14 and mSL-13 were designed to test how far from the A- and P-sites the ribosomal helicase site is located. They contain stem-loop structures with 15, 14, and 13 G-C base pairs, respectively, in which the first G-C pairs of the duplexes are placed at nucleotides +10, +11, and +12, respectively, where +1 is defined as the 5′ base of the Arginine codon, which serves as a reference location in the experiments below (Fig. 1 and Supplementary Table 1). mPK contains a pseudoknot modified from infectious bronchitis virus (IBV). We chose this pseudoknot and its variants following studies of Brierly et al. [8,16,17] who determined frameshifting efficiency as a function of pseudoknot structure. U7C, which exhibits similar

frameshifting efficiency to mPK, stabilizes the pseudoknot. In contrast, variants G3C G4C and G15C G42C, which weaken secondary structure relative to mPK, are not expected to induce frameshifting. mPK-SL, a single 17-bp stem loop with the same set of base pairs as mPK, but no stabilizing tertiary interactions, does not induce frameshifting [8,17]. The first base-pair of the pseudoknot structures in these mRNAs are located at nucleotide +12, defined as above. mSL-15e, mSL-14e and mSL-13e (Fig. 1), used in ensemble kinetic experiments described at the end of Results, contain stem-loop structures similar to mSL-15, mSL-14 and mSL-13.

We measured the dwell times of PRE and POST complexes that are formed as two elongation cycles add Arginine[8] and Phenylalanine[9] to the growing peptide, using three different smFRET measurements (Fig. 2): i) between two adjacent tRNAs bound to the ribosome [18,19]; ii) between tRNA and the large subunit protein, L11, near the A-site [18]; and iii) between tRNA and L1, near the E-site [20]. The PRE and POST complexes studied in these experiments are shown in Fig. 2. The POST complexes contained either just peptidyl-tRNA in the P-site [$POST^{E}$, peptidyl-$tRNA^{Glu}$ (complex ***1***); $POST^{R}$, peptidyl-$tRNA^{Arg}$ (***4***); or $POST^{F}$, peptidyl-$tRNA^{Phe}$ (***7***)], or deacylated tRNA in the E-site and peptidyl-tRNA in the P-site [$POST^{ER}$, $tRNA^{Glu}$/peptidyl-$tRNA^{Arg}$ (***3***); or $POST^{RF}$, $tRNA^{Arg}$/peptidyl-$tRNA^{Phe}$ (***6***)]. The PRE complexes contained peptidyl-tRNA in the A-site and deacylated tRNA in the P-site [PRE^{ER}, $tRNA^{Glu}$/peptidyl-$tRNA^{Arg}$ (***2***); or PRE^{RF}, $tRNA^{Arg}$/peptidyl-$tRNA^{Phe}$ (***5***)]. Fig. 2 also shows the fluorophore-labeled component(s) present in each complex and, qualitatively, the FRET efficiencies (blue halos) in the various complexes containing fluorophore pairs, which are in accord with previous results[18-20].

tRNA-tRNA smFRET

Unless otherwise indicated, all translation experiments began with 70S ribosome initiation complexes (ICs), programmed with mRNA and an fMet-$tRNA^{fMet}$ in the P-site, and immobilized in microscope slide flow chambers via biotin-streptavidin linkage at the 3′-end of the mRNA. We initiated translation by injecting into the flow cell a mixture of ternary complexes (aa-tRNA·EF-Tu·GTP, TCs) containing Cy3-labeled Arg-$tRNA^{Arg}$ (Cy3-R), Cy5-labeled Phe-$tRNA^{Phe}$ (Cy5-F), and unlabeled Tyr-$tRNA^{Tyr}$ and Glu-$tRNA^{Glu}$, and other necessary protein synthesis components. Two dwell times were measured from each fluorescence trace (Fig. 3A): the dwell time of the Cy3-only state, corresponding to the combined lifetimes of complexes ***2***–***3***–***4***, and the dwell time of the FRET state, corresponding to combined lifetimes of complexes ***5***–***6*** (Fig. 2, row B). Both dwell times are exponentially distributed (Fig. 3B and C), allowing determination of the overall rate constants for the conversion of PRE^{ER} (***2***) to PRE^{RF} (***5***) and of PRE^{RF} (***5***) to $POST^{F}$ (***7***) [Figs. 2 (row C) and 3], respectively. These rate constants are presented in Figs. 3D and 3E, and in Supplementary Table 2, for ribosomes programmed with each of the mRNAs studied. It is important to note that since the end of interval (***4***) is the beginning of interval (***5***), the reciprocal of the combined dwell times of complexes ***2***–***3***–***4*** gives the overall rate constant for (***2***) → (***5***) conversion. This nomenclature for dwell time distributions and the corresponding fitted rate constants is used for all of the intervals measured in this paper.

For ribosomes programmed with mRNAs mSL-13, mSL-14, and mSL-15, the rate constants for PRE^{ER} to PRE^{RF} conversion (***2*** → ***5***) are progressively decreased, from 49% to 57% to 64% relative to that for mRNA mPL (Fig. 3D and Supplementary Table 2), as the beginning of the stem-loop duplex is moved from the +15 position in mSL-13 (+1 is the first (5′) base of the P-site codon, Glutamate in this case) to the +14 and +13 position in mSL-13, mSL-14 and mSL-15, respectively. The progressive decrease of translation rate is consistent with the notion that, as expected, the number of base pairs disrupted in this cycle progressively increases from mSL-13 to mSL-14 to mSL-15. In contrast, the rate constants for PRE^{RF} to $POST^{F}$ conversion (***5*** → ***7***) are similar for mRNAs mSL-13, mSL-14 and mSL-15 (stem-loop duplex starting +12, +11 and +10 relative to +1, the 5′ base of the P-site codon, now Arginine) and 76% less than that of mRNA mPL (Fig. 3E), suggesting that all of these mRNAs have three stem-loop base pairs disrupted in this elongation cycle. Taken together, these results indicate that the closest intact mRNA base pair is located at 12 or 13 nucleotides (nts) downstream from 5′ base of the P-site codon, in accordance with previous estimates of +12 – +14 [11,14]. A further test of this distance was carried out using ensemble kinetics, which is presented at the end of Results.

We performed similar rate measurements on mPK, and on the four variants of mPK described above (Fig. 1). Compared to mRNA mPL, mPK and its four variants show relatively minor decreases in the rate constants for PRE^{ER} to PRE^{RF} conversion (***2*** → ***5***) (no more than a 40% decrease). The G3C G4C and G15C G42C variants, which have a two-base-pair mismatch in either stem 1 or stem 2, respectively, have almost the same rate as mPL. All of the mRNAs with 2° structures showed considerable (50% – 79%) decreases in the rate of PRE^{RF} to $POST^{F}$ conversion (***5*** → ***7***), except for the G3C G4C variant. These results support the conclusion that the melting of 2° structure starts at the +12 – +13 position downstream from the first base of the P-site.

L11-tRNA smFRET

We used FRET measurements between tRNA and either L11 or L1 to determine which specific steps within the elongation cycle are responsible for the lowered elongation rate constants presented in Fig. 3 and Supplementary Table 2. In our previous studies, we found that Cy5-labeled L11 (Cy5-L11) has strong FRET (E = 0.4–0.8) to Cy3-labeled tRNA in the A-site[18], and that L11-tRNA FRET is decreased markedly (to E = 0.2) on tRNA translocation. This signal can thus be used to measure the rates for delivery of aa-tRNA into the A-site, transitions between fluctuating PRE state conformations, and translocation from the PRE to the POST complex.

After preformed $POST^{E}$(***1***) complexes containing Cy5-L11 were immobilized, we injected 10 nM Cy3-R TC into flow chamber while recording the fluorescence intensities of Cy3 and Cy5 (due to FRET). The delay times measured from injection of Cy3-R into the flow chamber until appearance of steady Cy3 and FRET intensities were used to calculate apparent delivery rates of Cy3-R into the A-site of $POST^{E}$(***1***). Apparent delivery rates of Cy3-F into the A-site of $POST^{R}$(***4***) were measured similarly (Fig. 2, rows C and D and Supplementary Figure 1). The delay time between injecting the labeled tRNA and appearance of Cy3 and FRET intensity was ~7 s, corresponding mostly to second-order

binding of Cy3-R to the ribosome, with a 2nd-order rate constant of ~14 $\mu M^{-1}s^{-1}$ (= 1/(7 s × 10 nM Arg-$tRNA^{Arg}$)). The dead time during injection for the measurement (~0.1 s measured by increased intensity of background fluorescence) is relatively small. Comparison of rates of tRNA delivery for the various test mRNAs (Supplementary Figure 1 and Supplementary Table 2, columns ***1*** → ***2*** and ***4*** → ***5***) showed that the downstream mRNA 2° structures did not affect delivery rate of cognate tRNA into A-site, even when rates in the preceding elongation cycle were slowed (e.g. with mSL-15).

The PRE complex fluctuates between two major conformations, termed the classical and hybrid PRE states[21-23]. Using FRET between Cy5-L11 and Cy3 labeled peptidyl-tRNA in the A-site, the classical and hybrid PRE states are signaled as high and low FRET states [18,24] respectively, because the distance between the tRNA and L11 labeling sites is greater in the hybrid state. During a one-minute observation time, PRE complexes can either fluctuate between classical and hybrid states or remain in one of the states. Both fluctuating and non-fluctuating PRE complexes are active in translocation assays[18]. Using FRET between Cy5-L11 and Cy3-F in PRE^{RF} (***5***) complexes measured in the absence of EF-G, we found almost no effect of downstream mRNA 2° structures on the distribution between non-fluctuating and fluctuating PRE complexes, partitioning between the classical and hybrid states in both fluctuating and non-fluctuating complexes, or transition rates between fluctuating complexes (Supplementary Table 3). Overall, mRNA 2° structures did not affect fluctuating or non-fluctuating PRE complexes.

Monitoring the decrease of L11-tRNA FRET in the presence of EF-G·GTP (Fig. 2, rows C and D) provides a direct measure of the dwell time of the PRE complexes and thus of the rate constants for tRNA translocation within the 50S subunit. Translocation of PRE complexes to POST complexes reduces L11-tRNA FRET from 0.4–0.8 to 0.2 (Figs. 4 A and B) [18]. We measured the dwell times of PRE complexes prior to the transition to the 0.2 FRET state for both complexes PRE^{ER} (***2***) and PRE^{RF} (***5***), and calculated apparent translocation rates of PRE^{ER} to $POST^{ER}$ (***2*** → ***3***) and PRE^{RF} to $POST^{RF}$ (***5*** → ***6***) (Fig. 4), respectively. To our surprise, tRNA translocation rates on the 50S subunit in both elongation cycles were hardly affected by mPK or any of its variants (Figs. 4E, 4F, and Supplementary Table 2, columns ***2*** → ***3*** and ***5*** → ***6***) relative to mPL. A more nuanced result was obtained for the mSL variants, which hardly affected the rate of PRE^{ER} to $POST^{ER}$ (***2*** → ***3***) conversion, but, in each case, decreased the rate of PRE^{RF} to $POST^{RF}$ (***5*** → ***6***) conversion by ~ 50%. These results demonstrate that the unwinding of downstream pseudoknot or stem-loop 2° structures, which presumably accounts for the slowing of elongation (Fig. 3), is not rigidly coupled to tRNA translocation in the 50S subunit. In contrast, the results presented below indicate that it is dissociation of tRNA from the E-site that is invariably slowed when the ribosome encounters these 2° structures.

L1-tRNA smFRET

FRET measurements between Cy5-L1 and Cy3-R (Fig. 2, row E) allowed us to monitor both $tRNA^{Arg}$ movement within the ribosome and its dissociation from the E-site during elongation. We observed four distinct FRET states that occurred in the temporal sequence *E* = 0.07, 0.66, 0.40, and 0.78 (Fig. 5A). A density map for transitions between these states

(Supplementary Figure 2) shows that the temporal order among these states was largely unidirectional and highly consistent between traces. To help assign these states to $tRNA^{Arg}$ positions in the ribosome, experiments were conducted at an order of magnitude lower concentration (5 nM) of the next cognate ternary complex, F-TC, than the 50 nM concentration typically employed. The lower concentration slows association of F-TC and $POST^{R}$ (***4***) to form PRE^{RF}(***5***), thereby delaying translocation to form $POST^{RF}$(***6***). The dwell times of both 0.40 and 0.66 FRET states were markedly lengthened at 5 nM [F-TC] (dwell time histograms, Fig. 5B, and heat maps, Supplementary Figure 3A and B). Accordingly, these FRET values were assigned to the states containing Cy3-R in the P-site (complexes $POST^{ER}$ (***3***), $POST^{R}$ (***4***), and PRE^{RF}(***5***)). Reversible transitions between 0.40 and 0.66 FRET efficiency at low [F-TC] are the result of conformational dynamics of the L1 stalk and of the E-site and P-site tRNAs in complexes $POST^{ER}$ (***3***) and $POST^{R}$ (***4***) [25-27]. Pre-formed $POST^{R}$ (***4***) and PRE^{RF} (***5***) complexes each gave L1-tRNA FRET values of ~0.40, whereas addition of deacylated $tRNA^{Glu}$ to pre-formed $POST^{R}$ to form the $POST^{ER}$ complex (***3***) produced the 0.66 FRET state. Taken together, these results allow the 0.07, 0.66, 0.40, and 0.78 FRET states to be assigned to the complexes ***2***, ***3***, ***4***–***5***, and ***6***, respectively, in the two different elongation cycles. Although the absolute values of translation rates measured here with different FRET pairs do not exactly match each other (Supplementary Table 2), the trends and extent of slowing of the rates of specific steps affected by secondary structure (columns in Supplementary Table 2) are quite similar for the different FRET pairs.

Dissociation rates of $tRNA^{Glu}$ (***3*** → ***4***) and $tRNA^{Arg}$ (***6*** → ***7***) from the E-site were determined from the dwell times of the 0.66 and 0.78 FRET states, respectively (Fig. 5 and Supplementary Table 2). The results show that for both cycles the presence of a downstream stem-loop in mRNA of all G-C base pairs markedly decreases the rate of tRNA dissociation from the E-site. In the earlier cycle, mRNA mSL-13, mSL-14, and mSL-15 progressively decrease rates of $tRNA^{Glu}$ dissociation by 47% to 58% to 66% compared to mRNA mPL (Supplementary Table 2, column ***3*** → ***4***); in the later cycle, $tRNA^{Arg}$ dissociation rate is approximately halved for all three mSL structures (Supplementary Table 2, column ***6*** → ***7***). Although the stem-loops in the mSL variants (Fig. 1) do not affect the rate of translocation when encountered at positions +13 – +15 relative to 5′ -end of the P-site (+1) (Supplementary Table 2, column ***2*** → ***3***), they do markedly slow translocation at positions +10 – +12 (Supplementary Table 2, column ***5*** → ***6***).

Downstream pseudoknots also reduce the rate of $tRNA^{Arg}$ dissociation (***6*** → ***7***) when the first base-pair of mPK or its variants are at position +12, with the effects being larger for mPK, mPK-U7C, and mPK-SL (45–61% decrease) and less for the two mPK mutants with weakened 2° structure, but pseudoknots have virtually no effect on $tRNA^{Glu}$ dissociation (***3*** → ***4***) when the first base-pair is at position +15. The generalities that emerge from these results are that downstream 2° mRNA structures substantially reduce the dissociation rate of E-site tRNA, that this slowing accounts for the most of the observed rate reduction of the overall elongation cycle for the mRNA structures we have examined, and that the slowing effects are more common when 2° structure is encountered at positions +10 – +12 than further downstream (+13 – +15).

In both mRNA mPK and mPK-G15C G42C, conversion from PRE^{RF} (***5***) to $POST^{F}$ (***7***) requires unwinding of the same three G-C pairs at 5′ end of the 2° structures. However, mRNA mPK-G15C G42C slows elongation much less than mPK even though the mismatched base pairs in mPK-G15C G42C are located at the 3′ end of the pseudoknot, away from the segment entering the mRNA entry channel. It is possible that destabilization of the stem 2 structure in mPK-G15C G42C results in formation of a simple stem-loop structure with 11 base pairs, which can be more easily unfolded by the ribosome than the native mPK. Alternatively, the extra bulge in mPK-G15C G42C may inhibit untwisting of the 5′ stem during unfolding to a lesser extent than in mPK [28]. Although the three base pairs closest to the mRNA entry channel are all G-C pairs in both mPK-SL and the mSL mRNAs, reducing overall G-C content from 100% (SL series) to 65% (mPK-SL) removed inhibition of translocation from PRE^{RF} (***5***) to $POST^{RF}$ (***6***). These results suggest that cooperative mechanisms in 2° structures can modulate long-range interactions between base pairs [29].

2-1-2 vs. 2-3-2 pathway

The E-site tRNA in the POST complex dissociates either allosterically after the binding of aminoacyl-tRNA to the A-site (termed the 2-3-2 pathway), or spontaneously, and prior to binding of aminoacyl-tRNA to the A-site (termed the 2-1-2 pathway)[19]. Our previous studies on ribosomes programmed with mRNAs lacking stable downstream 2° structure showed the 2-1-2 pathway to be dominant after the first 3 – 4 elongation cycles. Consistent with these earlier results, here we found the 2-1-2 pathway to be dominant for $tRNA^{Arg}$ release from the $POST^{RF}$ complex programmed with mPL-mRNA, by two criteria. First, when reactions were carried out using Cy3-R and unlabeled ribosomes, 96 – 98% of the E-site Cy3-R molecules disappeared before the binding of the next incoming TC, Cy5-V-TC (Supplementary Figure 4). Second, the presence or absence of added 50 nM V-TC had no detectable effect on the rate constant for Cy3-R dissociation from the E-site (0.38 ± 0.01 s^{-1} *vs.* 0.39 ± 0.01 s^{-1}). Similar results were obtained for ribosomes programmed with mPK, mPK-SL, and mSL-15 (Table 1). The contribution of photobleaching in these conditions to disappearance of the fluorescent signal from the ribosome was determined to be less than 2% [19]. These results indicate that, despite the increased tRNA residence time at the E-site that is a consequence of downstream 2° mRNA structure, tRNA dissociation from the E-site still precedes cognate TC complex binding to the A-site: i.e., the 2-1-2 pathway is maintained.

Ensemble experiments

We also carried out ensemble stopped-flow experiments to measure the effect of downstream stem-loop structures on elongation cycle kinetics[30]. PRE complexes programmed with mRNAs mSL-15e, mSL-14e and mSL-13e (Fig. 1) contained proflavin(prf)-labeled peptidyl-$tRNA^{Arg}$ in the A-site, $tRNA^{Phe}$ in the P-site, and a G-C stem-loop at positions +13, +14, and +15 nts, respectively. Upon rapid mixing of the PRE complexes with EF-G·GTP, proflavin fluorescence intensity increased and then decreased more slowly, allowing calculation of two apparent rate constants (k_{app1} and k_{app2}, Supplementary Figure 5). The fast phase, which is beyond the time resolution of our smFRET measurements, is due to a conformational change in the ribosome after GTP hydrolysis by EF-G and precedes tRNA movement. The second slower phase is caused by

both translocation and dissociation of tRNA from the E-site. Results at different EF-G concentrations, summarized in Table 2, show that both phases are progressively slowed as the stem-loop is brought closer to the A- and P-sites, leading to ~80% decreases in both k_{app1} (37 s^{-1} to 8 s^{-1}) and k_{app2} (1.4 s^{-1} to 0.25 s^{-1}) for mSL-15e compared with mSL-13e at 4 μM EF-G, which is close to saturating [EF-G]. These results support the conclusion from the smFRET results and earlier studies [11,14] that the base of the stem-loop is 12 or 13 mRNA nts downstream from the 5′ end of the P-site just prior to unwinding.

Discussion

Previous single molecule optical trap experiments measured the effects of downstream 2° mRNA structure on polypeptide elongation rate without resolving rates of sub-steps in the elongation cycle [14,15]. The overall rate of elongation in the present experiments is consistent with these earlier studies when the lower tRNA concentrations imposed by fluorescence background here are considered, as described in the notes with Supplementary Table 2. Their results have been interpreted based on the assumption that helix melting necessarily accompanies the translocation step [14,15]. Thus, an unexpected feature of our results is that the step in the elongation cycle most consistently affected by downstream secondary structure is E-site tRNA release, rather than translocation of the tRNAs relative to the 50S subunit. This indicates that melting of the RNA duplex at the helicase site takes place mainly after tRNA translocation and before or concomitant with E-site tRNA dissociation. Translocation was measured by changes in the fluorescence of tRNAs labeled within their D-loops [31] that monitor the movement of tRNAs within the large subunit. Movements of mRNA and tRNA in the small subunit were not directly monitored. Since ensemble studies have shown that the overall rates of tRNA and mRNA translocation are equal to one another [32,33], our results may suggest that the distance from the tRNA binding sites to the mouth of the mRNA entry channel, which for most of the mRNAs we employ is also the edge of the unmelted mRNA 2° structure, contracts during translocation and extends again before or during E-site tRNA dissociation. Such a structural change would allow translocation without concomitant unwinding of the mRNA. Alternatively, transient movement of some unmelted secondary structure into the mRNA channel cannot be excluded, given recent cryoelectron microscopy results demonstrating substantial opening of the channel during translocation of ribosome-bound tmRNA[34] due to the movement of protein S3 at the channel entrance.

An alternative interpretation of our results is that the intermediate state we detect after tRNA translocation corresponds to full translocation of tRNAs in the large subunit but no mRNA or tRNA movements in the small subunit. Then tRNA release from the E-site would occur either simultaneously with mRNA motion in the small subunit and 2° structure unwinding or in a rapid step following unwinding and 30S translocation. Results presented in Supplementary Table 3 indicate that the dynamics of tRNA movements during transitions between the classical and hybrid PRE states [21,22] are not affected by mRNA 2° structure. tRNAs would thus have to bend far more than in the hybrid state to allow further motion in the 50S subunit uncoupled to translocation in the 30S subunit. Such bending is, at least plausible, based on cryoelectron microscopy results demonstrating the presence of tRNAs

severely bent in the required direction in eukaryotic ribosomes stalled by the same IBV pseudoknot used in the present work [5].

In the two interpretations presented above, the movements of mRNA and tRNAs in the small subunit accompanying translocation of tRNAs in the large subunit are either completed or negligible. An intermediate possibility is that complete translocation of tRNAs in the large subunit is accompanied by a partial translocation in the small subunit, forming an intermediate in which deacylated tRNA interacts with the E-site in the large subunit and both E- and P-sites in the small subunit, as has recently been suggested from cryo-EM images of translocation intermediates stalled on the ribosome by the antibiotic fusidic acid [34,35]. Distortion of the tRNAs in both of these studies moves their D-loops several nm farther from L11, as we have observed (Fig. 4), and such movement could occur prior to mRNA translocation within the 30S subunit. Irrespective of which of these detailed interpretations is correct, our results clearly show that the mRNA entry channel allosterically interacts with the E-site to modulate tRNA dissociation when the ribosome encounters mRNA 2° structures. Such communication could be achieved by large scale conformational changes within the ribosome on completion of an elongation cycle, reverse ratcheting [36] and/or reverse swiveling of the 30S head with respect to the 30S body [35].

We chose the pseudoknot studied here and its variants following studies of Brierly et al. [16,17] who determined frameshifting efficiency as a function of pseudoknot structure. U7C, which exhibits similar frameshifting efficiency to mPK, stabilizes the pseudoknot. In contrast, G3C G4C and G15C G42C, which weaken secondary structure, are expected to show diminished frameshifting efficiency. As anticipated, there is a clear correlation between the propensity of pseudoknot structures and their variants to induce frameshifting, as measured by others [16,17], and their tendency to slow E-site $tRNA^{Arg}$ dissociation (Supplementary Table 4). The exception is mPK-SL, which shows similar kinetics to those of mPK in our experiments, but does not induce frameshifting in eukaryotes [17]. As suggested by Somogyi et al. [17], it is possible that some feature of the pseudoknot beyond its ability to pause elongation is important for its induction of frameshifting.

Duplex unwinding by the ribosomal helicase has been shown to proceed via two mechanisms, one involving thermal ratcheting of a partially open form of the stem which exists in rapid equilibrium with the closed form, while the other one requires free-energy released as a consequence of GTP hydrolysis and/or peptide bond formation to forcibly unwind the stem [14]. Our observation that both tRNA translocation and E-site tRNA dissociation can be slowed by secondary structures leads us to speculate that the two steps may utilize different unwinding mechanisms, although which mechanism would be favored for each step is not known.

Conclusions

In this study, we examined how downstream mRNA 2° structures modulate the kinetics of ribosomes during translation. Using tRNA-tRNA, L11-tRNA and L1-tRNA FRET pairs, we measured rate constants for delivery of ternary complexes into the A-site, translocation of tRNAs in the 50S subunit, and dissociation of E-site tRNAs during elongation cycles when

such 2° structures were present at the entrance of the mRNA channel. Stem loops containing 100% G-C pairs lead to 45–66% decreases in both the translocation and E-site tRNA dissociation steps suggesting that, when necessary, the ribosome applies two sequential helicase actions within each elongation cycle to unwind duplex mRNA. On the other hand, stable stem loops and pseudoknots containing both G-C and A-U pairs only slow E-site tRNA dissociation, suggesting that in these cases 30S translocation of the tRNAs and unwinding of 2° structures are decoupled. Neither stem-loops nor pseudoknots affect the delivery rate of cognate tRNA into the A-site or dynamics of tRNAs between the classical and hybrid PRE states. Our results indicate that, in most cases, the presence of a stable downstream mRNA 2° structure at the entrance to the mRNA channel prolongs the lifetime of POST translocation complexes containing tRNAs in both the E- and the P-sites.

Online methods

Ribosome preparation

Unlabeled 70S, 70S with Cy5-labeled L11 (70S-L11^{Cy5}), 50S with Cy5-labeled L1 (50S-L1^{Cy5}), and 30S ribosomes were prepared according to published procedures [18,20,37,38]. For tRNA-tRNA and L11-tRNA FRET experiments, initiation complexes were formed by mixture of 70S or 70S-L11^{Cy5} ribosomes with mRNA, initiation factors, and fMet-tRNAf^{Met} in TAM$_{15}$ buffer (37 °C, 25 min), and purified by centrifugation through a sucrose cushion [18]. For L1-tRNA experiments, 50S-L1^{Cy5} subunit was combined with purified 30S subunits at 42 °C for 10 min in order to form 70S-L1^{Cy5} ribosomes, prior to mixing with mRNA, initiation factors and fMet-tRNA^{fMet} to prepare 70S initiation complexes.

Charged and Labeled tRNA preparation

Amino acid specific tRNAs, *E. coli* tRNA^{fMet}, *E. coli* tRNA^{Tyr}, *E. coli* tRNA^{Glu}, *E. coli* tRNA^{Arg}, yeast tRNA^{Phe}, *E. coli* tRNA^{Val} were purchased from Chemical Block, Inc. (Moscow) and prepared using the reduction, charging and labeling protocol as described [31,39]. Neither the charging nor the labeling reactions went to completion. Partial separation of charged from uncharged tRNAs was achieved by reverse-phase HPLC using a LiChrospher WP-300 RP-18 column (5 μm beads, 250 × 4 mm, Merck KGaA-Darmstadt). The tRNA mixture was applied to the column equilibrated with buffer A (20 mM NH_4Ac pH 5.0, 10 mM $MgAc_2$ and 400 mM NaCl) and the aminoacylated tRNAs were eluted with a linear gradient of buffer A containing 30% (v/v) ethanol. Cy3/Cy5 labeled tRNAs were fully resolved from unlabeled tRNAs using the same column and buffers, but at a higher pH (7.0) with elution at 10 °C instead of room temperature. Stoichiometries of fluorophore/tRNA labeling varied from 0.7 – 1.2 probe per tRNA[31]. Ternary complexes were formed by incubating 2 μM EF-Tu, 1 μM charged tRNAs, 3 mM GTP, 1.3 mM phosphoenolpyruvate, and 5 μg/mL pyruvate kinase in TAM[15] buffer for 15 min at 37 °C.

mRNA preparation

mRNAs for smFRET experiments were prepared via *in vitro* transcription and 3′-biotinylation. DNA fragments corresponding to mRNAs were cloned into a pTZ18R vector, which contains a T7 promoter, through the SLIM PCR method [40]. The DNA sequence in the

coding region was confirmed by sequencing. The DNA construct was linearized with Hind III and used as a template for transcription using the AmpliScribe T7-Flash *in vitro* Transcription Kit (Epicentre). The transcript was purified via phenol and chloroform extraction, followed by precipitation with 5 M LiCl and 95% Ethanol. The final RNA sample was dissolved in DEPC-treated H_2O. The integrity and purity of the mRNA was confirmed using agarose gel electrophoresis.

The mRNA biotinylation procedure was modified from a previous procedure [41], based on selective periodate oxidation of RNA at its 3′ end and reaction of the oxidized product with biotin hydrazide. Typically, the oxidation of mRNA was performed in a solution containing mRNA (10 – 50 A_{260}/ml), 100 mM sodium acetate (pH 5.0) and 90 mM sodium m-periodate (prepared fresh). After an incubation of 2 hours at room temperature, periodate was precipitated by adding KCl to a final concentration of 200 mM and incubating for 5 minutes on ice. The precipitate was removed by centrifugation for 5 minutes at 10,000g, 2 °C and passage of the supernatant through a Sephadex G-25 column (Nap-5, Pharmacia). Biotin hydrazide (21339, Pierce) was then added to a final concentration of 2 mM from a 50 mM stock in DMSO (prepared fresh). Biotinylation was carried out for 2 hours at room temperature, after which the mixture was put through a Sephadex G-25 column (PD-10, Pharmacia). Biotinylated mRNA was precipitated by ethanol addition and dissolved in DEPC-treated H_2O. The concentration of biotinylated mRNA was determined by A_{260}.

Acquisition and analysis of smFRET data

Initiation complexes were specifically attached to microscope flow cells via biotinylated mRNA to PEG-passivated slides, decorated with biotin-PEG and streptavidin. smFRET experiments were performed in TAM_{15} buffer (15 mM $MgAc_2$, 50 mM Tris-HCl pH 7.5, 30 mM NH_4Cl, 70 mM KCl, and 1 mM dithiothreitol) with an oxygen scavenging system (3 mg/mL glucose, 100 μg/mL glucose oxidase (Sigma-Aldrich), 40 μg/mL catalase (Roche), and 1.5 mM 6-hydroxy-2,5,7,8-tetramethyl-chromane-2-carboxylic acid (Trolox, Sigma-Aldrich – added from a concentrated DMSO stock solution). Ensemble experiments were performed in buffer B containing 50 mM Tris-HCl (pH 7.5), 70 mM NH_4Cl, 30 mM KCl, 7 mM $MgCl_2$ and 1 mM dithiothreitol.

Single molecule spectroscopic microscopy was performed on a home-built objective-type TIRF microscope, based on a Nikon Eclipse Ti with an EMCCD camera (Photometrics Cascade 512b), and solid state 532 nm and 640 nm excitation lasers, as described before [18]. For tRNA-tRNA experiments, alternating excitation between 532 nm and 640 nm excitation [42] was achieved with an acousto-optic tunable filter (AOTF, AA Opto-Electronic, Inc.) synchronized with the camera. Fluorescence emission from the probes was collected by the microscope and spectrally separated by interference dichroic (630 nm) and bandpass filters, 585/70 nm (Cy3) and 680/50 nm (Cy5), in a Dual-View spectral splitter (Photometrics, Inc., Tucson, AZ).

Collection of real-time translation traces began 10 s prior to injecting 10 nM labeled ternary complexes, 50 nM unlabeled ternary complexes, 2 μM EF-G, and 2 mM GTP into flow chambers containing initiation complexes, and was carried out without further washing. All

FRET traces were analyzed by a Hidden Markov Model based software package [HaMMy [43]] and dwell times of FRET states were extracted from the HaMMy analysis.

Supplementary Material

Refer to Web version on PubMed Central for supplementary material.

Acknowledgements

Supported by US National Institutes of Health grant R01GM080376 to B.S.C. and Y.E.G. and American Heart Association Postdoctoral Fellowship 12POST8910014 to C.C.

References for main text

1. Zhang G, Hubalewska M, Ignatova Z. Transient ribosomal attenuation coordinates protein synthesis and co-translational folding. Nat Struct Mol Biol. 2009; 16:274–280. [PubMed: 19198590]
2. Guisez Y, Robbens J, Remaut E, Fiers W. Folding of the Ms2 coat protein in Escherichia-Coli is modulated by translational pauses resulting from messenger-RNA secondary structure and codon usage - a hypothesis. J Theor Biol. 1993; 162:243–252. [PubMed: 8412226]
3. Varenne S, Buc J, Lloubes R, Lazdunski C. Translation is a non-uniform process - effect of transfer-RNA availability on the rate of elongation of nascent polypeptide-chains. J Mol Biol. 1984; 180:549–576. [PubMed: 6084718]
4. Kimchi-Sarfaty C, et al. A “silent” polymorphism in the MDR1 gene changes substrate specificity. Science. 2007; 315:525–528. [PubMed: 17185560]
5. Namy O, Moran SJ, Stuart DI, Gilbert RJC, Brierley I. A mechanical explanation of RNA pseudoknot function in programmed ribosomal frameshifting. Nature. 2006; 441:244–247. [PubMed: 16688178]
6. Giedroc DP, Cornish PV. Frameshifting RNA pseudoknots: Structure and mechanism. Virus Res. 2009; 139:193–208. [PubMed: 18621088]
7. Gurvich OL, et al. Sequences that direct significant levels of frameshifting are frequent in coding regions of Escherichia coli. Embo J. 2003; 22:5941–5950. [PubMed: 14592990]
8. Brierley I, Meredith MR, Bloys AJ, Hagervall TG. Expression of a coronavirus ribosomal frameshift signal in Escherichia coli: Influence of tRNA anticodon modification on frameshifting. J Mol Biol. 1997; 270:360–373. [PubMed: 9237903]
9. Brierley I, Dos Ramos FJ. Programmed ribosomal frameshifting in HIV-1 and the SARS-CoV. Virus Res. 2006; 119:29–42. [PubMed: 16310880]
10. Yusupova GZ, Yusupov MM, Cate JHD, Noller HF. The path of messenger RNA through the ribosome. Cell. 2001; 106:233–241. [PubMed: 11511350]
11. Takyar S, Hickerson RP, Noller HF. mRNA helicase activity of the ribosome. Cell. 2005; 120:49–58. [PubMed: 15652481]
12. Spahn CMT, et al. Structure of the 80S ribosome from Saccharomyces cerevisiae tRNA-ribosome and subunit-subunit interactions. Cell. 2001; 107:373–386. [PubMed: 11701127]
13. Barbara PF. Single-molecule spectroscopy. Accounts Chem Res. 2005; 38:503–503.
14. Qu XH, et al. The ribosome uses two active mechanisms to unwind messenger RNA during translation. Nature. 2011; 475:118–121. [PubMed: 21734708]
15. Wen JD, et al. Following translation by single ribosomes one codon at a time. Nature. 2008; 452:598–603. [PubMed: 18327250]
16. Brierley I, Rolley NJ, Jenner AJ, Inglis SC. Mutational analysis of the RNA pseudoknot component of a coronavirus ribosomal frameshifting signal. J Mol Biol. 1991; 220:889–902. [PubMed: 1880803]
17. Somogyi P, Jenner AJ, Brierley I, Inglis SC. Ribosomal pausing during translation of an RNA pseudoknot. Mol Cell Biol. 1993; 13:6931–6940. [PubMed: 8413285]

18. Chen CL, et al. Single-molecule fluorescence measurements of ribosomal translocation dynamics. Mol Cell. 2011; 42:367–377. [PubMed: 21549313]
19. Chen CL, et al. Allosteric vs. spontaneous exit-site (E-site) tRNA dissociation early in protein synthesis. PNAS. 2011; 108:16980–16985. [PubMed: 21969541]
20. Stevens B, et al. FRET-based identification of mRNAs undergoing translation. PLoS ONE. 2012; 7:e38344. [PubMed: 22693619]
21. Agirrezabala X, et al. Visualization of the hybrid state of tRNA binding promoted by spontaneous ratcheting of the ribosome. Mol Cell. 2008; 32:190–197. [PubMed: 18951087]
22. Julian P, et al. Structure of ratcheted ribosomes with tRNAs in hybrid states. 2008; 105:16924–16927.
23. Frank J, Gonzalez RL. Structure and dynamics of a processive brownian motor: The translating ribosome. Annu Rev Biochem. 2010; 79:381–412. [PubMed: 20235828]
24. Munro JB, Sanbonmatsu KY, Spahn CMT, Blanchard SC. Navigating the ribosome's metastable energy landscape. Trends Biochem Sci. 2009; 34:390–400. [PubMed: 19647434]
25. Fei J, Kosuri P, MacDougall DD, Gonzalez RL. Coupling of ribosomal L1 stalk and tRNA dynamics during translation elongation. Mol Cell. 2008; 30:348–359. [PubMed: 18471980]
26. Munro JB, et al. Spontaneous formation of the unlocked state of the ribosome is a multistep process. PNAS. 2010; 107:709–714. [PubMed: 20018653]
27. Cornish PV, et al. Following movement of the L1 stalk between three functional states in single ribosomes. PNAS. 2009; 106:2571–2576. [PubMed: 19190181]
28. Giedroc DP, Theimer CA, Nixon PL. Structure, stability and function of RNA pseudoknots involved in stimulating ribosomal frameshifting. J Mol Biol. 2000; 298:167–185. [PubMed: 10764589]
29. Rinnenthal J, Klinkert B, Narberhaus F, Schwalbe H. Direct observation of the temperature-induced melting process of the Salmonella fourU RNA thermometer at base-pair resolution. Nucleic Acids Res. 2010; 38:3834–3847. [PubMed: 20211842]
30. Pan DL, Kirillov SV, Cooperman BS. Kinetically competent intermediates in the translocation step of protein synthesis. Mol Cell. 2007; 25:519–529. [PubMed: 17317625]
31. Kaur J, Raj M, Cooperman BS. Fluorescent labeling of tRNA dihydrouridine residues: Mechanism and distribution. RNA. 2011; 17:1393–1400. [PubMed: 21628433]
32. Liu HQ, Pan DL, Pech M, Cooperman BS. Interrupted catalysis: The EF4 (LepA) effect on back-translocation. J Mol Biol. 2010; 396:1043–1052. [PubMed: 20045415]
33. Savelsbergh A, et al. An elongation factor G-induced ribosome rearrangement precedes tRNA-mRNA translocation. Mol Cell. 2003; 11:1517–1523. [PubMed: 12820965]
34. Ramrath DJF, et al. The complex of tmRNA-SmpB and EF-G on translocating ribosomes. Nature. 2012; 485:526–U140. [PubMed: 22622583]
35. Ratje AH, et al. Head swivel on the ribosome facilitates translocation by means of intra-subunit tRNA hybrid sites. Nature. 2010; 468:713–U143. [PubMed: 21124459]
36. Ermolenko DN, Noller HF. mRNA translocation occurs during the second step of ribosomal intersubunit rotation. Nat Struct Mol Biol. 2011; 18:457–462. [PubMed: 21399643]
37. Rodnina MV, Wintermeyer W. GTP consumption of elongation-factor Tu during translation of heteropolymeric messenger-RNAs. Proc. Natl. Acad. Sci. USA. 1995; 92:1945–1949. [PubMed: 7892205]
38. Subramanian AR, Dabbs ER. Functional-studies on ribosomes lacking protein L1 from mutant Escherichia-coli. Eur. J. Biochem. 1980; 112:425–430. [PubMed: 7007045]
39. Pan DL, Qin HO, Cooperman BS. Synthesis and functional activity of tRNAs labeled with fluorescent hydrazides in the D-loop. RNA. 2009; 15:346–354. [PubMed: 19118261]
40. Chiu J, Marc PE, Lee R, Tillett D. Site-directed, ligase-independent mutagenesis (SLIM): a single-tube methodology approaching 100% efficiency in 4 h. Nucleic Acids Res. 2004; 32
41. Odom OW, et al. Distances between 3' ends of ribosomal ribonucleic-acids reassembled into Escherichia-coli ribosomes. Biochemistry. 1980; 19:5947–5954. [PubMed: 6162473]

42. Kapanidis AN, et al. Fluorescence-aided molecule sorting: Analysis of structure and interactions by alternating-laser excitation of single molecules. Proc. Natl. Acad. Sci. USA. 2004; 101:8936–8941. [PubMed: 15175430]

43. McKinney SA, Joo C, Ha T. Analysis of single-molecule FRET trajectories using hidden Markov modeling. Biophys. J. 2006; 91:1941–1951. [PubMed: 16766620]

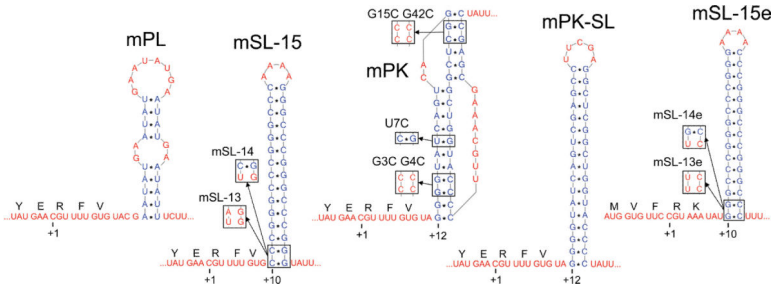

Fig. 1.

mRNA designators used in this study and their secondary structures. Positions of mRNA structures are indicated, defining the 5′-base of the Arginine codon as +1 (mRNA sequences are in Supplementary Table 1). M, R, F, V, K, Y, and E are single-letter abbreviations for N-formylmethionine, Arginine, Phenylalanine, Valine, Lysine, Tyrosine, and Glutamate, respectively. Base pairs are indicated in blue, whereas unpaired bases are indicated in red. Boxes and arrows indicate the mutations. At 23 °C, the most stable structure of mPL (ΔG = –5.6 kcal/mol, Supplementary Table 1) is far less stable than the structures of mPK-SL (ΔG = –37.1 kcal/mol) and mSL-15 (ΔG = –42.6 kcal/mol).

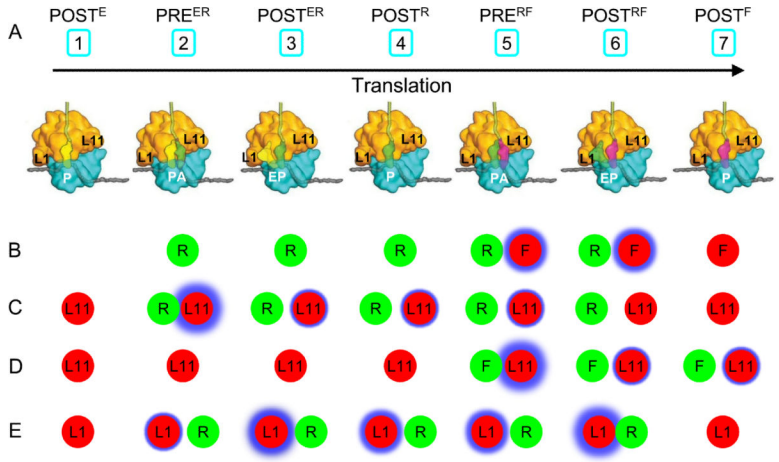

Fig. 2.

FRET studies on complexes formed through two elongation cycles that add Arginine and Phenylalanine to the nascent peptide. (**A**) Names and numerical designations of complexes. PRE and POST stand for pre-translocation and post-translocation complexes, respectively. E, R, and F are single-letter abbreviations for Glutamate, Arginine, and Phenylalanine, respectively. L11 and L1 are two large subunit ribosomal proteins. E, P, and A are the three tRNA binding sites on the ribosome. (**B**–**E**) smFRET experiments employed: Cy3-labeled Arg-tRNA^{Arg} (Cy3-R) and Cy5-labeled Phe-tRNA^{Phe} (Cy5-F) (**B**); Cy3-R or Cy3-labeled Phe-tRNA^{Phe} (Cy3-F) and Cy5-L11 (**C** and **D**); Cy3-R and Cy5-L1 (**E**). Labeled green and red dots indicate Cy3- and Cy5-labeled components, respectively. The thickness of the blue halo around the red dots qualitatively indicates the expected FRET efficiency.

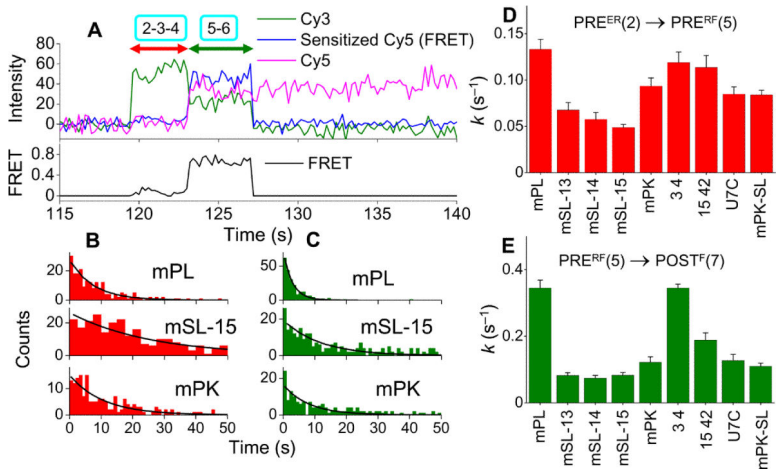

Fig. 3.

tRNA-tRNA smFRET. (**A**) Typical real-time ribosome translation trace measured using Cy3-R and Cy5-F, for ribosomes programmed with mPL. In addition to Cy3 fluorescence (green) and sensitized emission of Cy5 (FRET, blue) under 532 nm excitation, Cy5 direct fluorescence (magenta) was collected under alternating 640 nm laser excitation. Camera recording was started 10 seconds prior to injection of 10 nM Cy3-R and Cy5-F ternary complexes, 50 nM unlabeled Y and E ternary complexes, 2 μM EF-G, and 2 mM GTP and continued for 10 minutes at 100 ms integration time per frame. (**B** and **C**) Dwell time distributions of ribosome complexes programmed with different mRNAs (mPL, mSL-15, mPK) containing either Cy3-R only (**B**, complexes 2–4) or Cy3-R and Cy5-F, giving rise to FRET (**C**, complexes 5 and 6), respectively, fitted with single exponential decay curves (black lines), to give apparent rate constants for conversion of PRE^{ER} (complex 2) to PRE^{RF} (complex 5) and of PRE^{RF} (complex 5) to $POST^{F}$ (complex 7), respectively. In each case, times were collected from 200-400 ribosomes. (**D** and **E**) Apparent rate constants for steps from PRE^{ER} to PRE^{RF} (**D**) and from PRE^{RF} to $POST^{F}$ (**E**) for ribosomes programmed with the indicated mRNAs (including mPK-G3C G4C (3 4) and mPK-G15C G42C (15 42)). Error bars represent S.E.M., n ≥ 173.

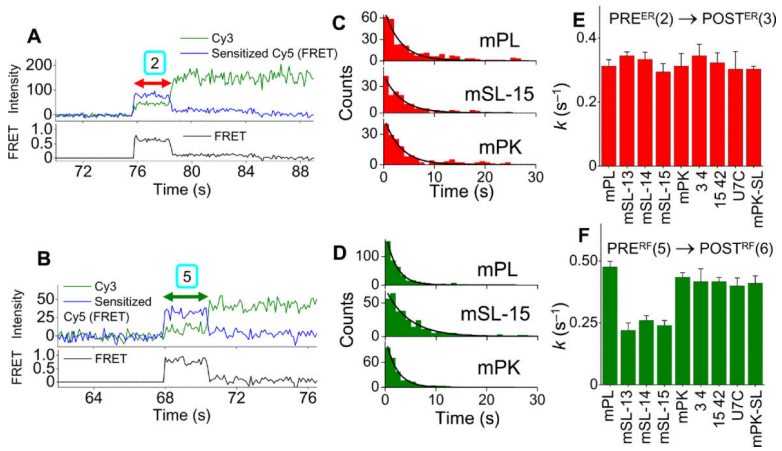

Fig. 4.

L11-tRNA smFRET. (**A** and **B**) Typical real-time ribosome translation traces measured using Cy3-R and Cy5-L11 (**A**) or Cy3-F and Cy5-L11 (**B**), for ribosomes programmed with mPL in the presence of 2 μM EF-G·GTP. Cy3 fluorescence (green) and sensitized emission of Cy5 (FRET, blue) under 532 nm excitation were collected. (**C** and **D**) Dwell time distributions of PRE^{ER} complexes (**C**; complex 2) and PRE^{RF} complexes (**D**; complex 5) from L11-tRNA measurements. (**E** and **F**) Apparent translocation rates of PRE^{ER} (**E**) and PRE^{RF} (**F**) complexes, respectively, from single exponential fitting (black curves) of dwell times of PRE^{ER} (**C**) and PRE^{RF} (**D**). Camera settings and abbreviations for mRNAs are as in Fig. 3. Error bars represent S.E.M., n ≥ 181.

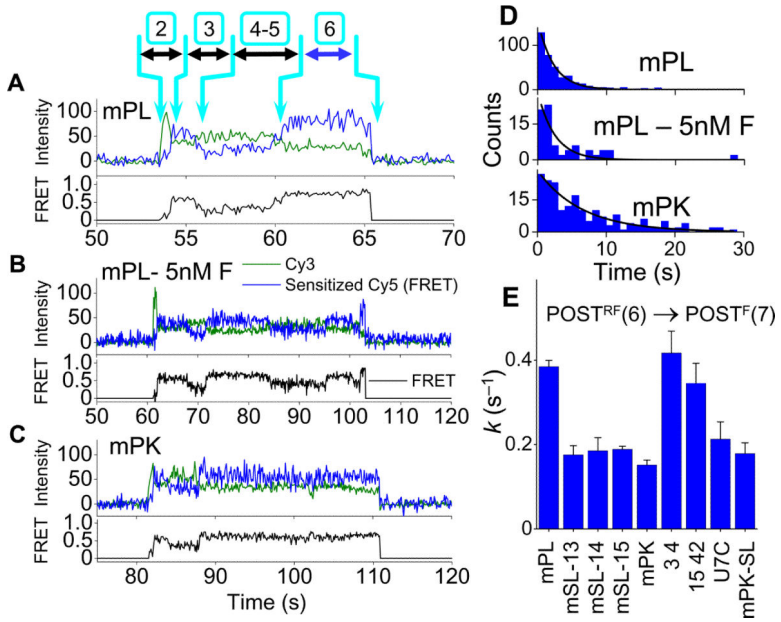

Fig. 5.

L1-tRNA smFRET. (**A**–**C**) Typical real-time ribosome translation traces measured using Cy5-L1 and 10 nM Cy3-R TC with mRNA mPL in the presence of 50 nM F-TC (**A**), 5 nM F-TC (**B**), and mRNA mPK at 50 nM F-TC (**C**). Traces and recording conditions are as in Fig. 4. (**D**) Dwell time distributions of $POST^{RF}$ complexes (complex 6) from L1-tRNA measurements. Unlabeled TC concentrations were 50 nM unless indicated. (**E**) Apparent dissociation rates of Cy3-R from the E-site were calculated from single exponential fitting (black curves) of dwell time of $POST^{RF}$ complexes (**D**). Error bars represent S.E.M., n ≥ 129.

Table 1

Distribution of translation pathways of the POST^{RF} complex with different mRNAs

mRNA	concentration of Cy5-V TC (nM)	Number of events	percentage of 2-1-2 pathway	Cy5-V TC association rate (s^{-1})[a]
mPL	10	157	97	0.12±0.02
mPK	10	96	98	0.10±0.02
mPK	20	157	94	0.18±0.03
mPK-SL	10	149	96	0.08±0.02
mSL-15	10	92	97	0.10±0.02

[a] S.E.M. are indicated. The contribution of photobleaching to disappearance of the fluorescent signal from the ribosomes was determined to be less than 2%[19].

Table 2

Ensemble measurements of translocation rate

Translocation	# cleaved bps	k_{app1} (s^{-1})[a] [EF-G], 1 μM 2 μM 4 μM	k_{app2} (s^{-1})[a] [EF-G], 1 μM 2 μM 4 μM
mSL-13e (cycle 4)	0	24 ± 1 26 ± 2 37 ± 3	0.60 ± 0.05 1.10 ± 0.05 1.41 ± 0.05
mSL-14e (cycle 4)	1	9.6 ± 0.3 16 ± 1 14 ± 1	0.43 ± 0.02 0.49 ± 0.02 0.65 ± 0.02
mSL-15e (cycle 4)	2	5.5± 0.1 7.6± 0.2 7.9 ± 0.2	0.21 ± 0.04 0.28 ± 0.03 0.25 ± 0.03

[a] S.E.M. are indicated.